

Statistical modeling of ultrasound signals related to the packing factor of wave scattering phenomena for structural characterization

François Destrempes^{a)} and Guy Cloutier^{b)}

Laboratory of Biorheology and Medical Ultrasonics, University of Montreal Hospital Research Centre (CRCHUM),
 900 St-Denis (suite R11.720), Montreal, Quebec, H2X 0A9, Canada

ABSTRACT:

The two-dimensional homodyned K-distribution has been widely used to model the echo envelope of ultrasound radio frequency (RF) signals in the field of medical ultrasonics. The main contribution of this work is to present a theoretical framework for supporting this model of the echo envelope and statistical models of the RF signals and their Hilbert transform in the case in which the scatterers' positions may be dependent. In doing so, the law of large numbers, Lyapounov's central limit theorem, and the Berry-Esseen theorem are being used. In particular, the proposed theoretical framework supports a previous conjecture relating the scatterer clustering parameter of the homodyned K-distribution to the packing factor W , which is related to the spatial organization of the scatterers, appearing in statistical physics or backscatter coefficient modeling. Simulations showed that the proposed modeling is valid for a number of scatterers and packing factors varying by steps of 2 from 1 to 21 and 1 to 11, respectively. The proposed framework allows, in principle, the detection of the structural information taking place at a scale smaller than the wavelength based solely on the statistical analysis of the RF signals or their echo envelope, although this goal was previously achieved based on the spectral analysis of ultrasound signals. © 2021 Acoustical Society of America.

<https://doi.org/10.1121/10.0007047>

(Received 27 May 2021; revised 1 October 2021; accepted 13 October 2021; published online 11 November 2021)

[Editor: James F. Lynch]

Pages: 3544–3556

I. INTRODUCTION

The homodyned K-distribution was introduced by Jakeman *et al.* as a generalization of the K-distribution¹ in the context of weak scattering.^{2,3} Applications of this statistical distribution have appeared in several fields, including optical propagation through turbulent media, microwave sea echo, land clutter, synthetic aperture radar imaging, and medical ultrasonics; see the references in Destrempes *et al.*⁴ However, this work is focusing on its applications in medical ultrasonics. The two-dimensional (2D) homodyned K-distribution was introduced in ultrasound imaging by Dutt and Greenleaf.⁵ Since then, the homodyned K-distribution has been adopted as a general statistical model for the echo envelope of ultrasound radio frequency (RF) signals by several research groups; see the references in Destrempes and Cloutier.⁶ Meanwhile, the one-dimensional (1D) K-distribution was proposed as a model for the absolute value of the RF ultrasound signals by Bernard *et al.*⁷

The homodyned K-distribution has one scaling parameter (the mean intensity, herein denoted μ) and two shape parameters: the scatterer clustering parameter, herein denoted by α ,

and the coherent-to-diffuse signal ratio,⁵ which is denoted by k . The shape parameter k is related to the diffuse-to-total signal power ratio⁸ $1/(\kappa + 1)$ as $\kappa = k^2/2$ and the coherent component⁹ ε of the homodyned K-distribution as $\varepsilon^2 = \mu k^2/(k^2 + 2)$. Whereas a physical interpretation of the parameters ε^2 and μ [and, hence, parameter $1/(\kappa + 1) = (\mu - \varepsilon^2)/\mu$] was proposed in Destrempes *et al.*,⁸ a physical interpretation of the shape parameter remained to be developed. It has been mentioned that the parameter α is equal to the average number $\langle N \rangle$ of scatterers per resolution cell.^{5,10} However, the results of a study on fatty duck livers¹¹ suggested that this parameter might also depend on the spatial organization of scatterers within the tissue. More precisely, in a recent work,⁶ we conjectured that parameter α can be interpreted as $\langle N \rangle/W$, where W is the packing factor introduced by Twersky.¹² The latter quantity arises from the statistical physics of fluids¹³ and may be defined as $\text{Var}[N]/\langle N \rangle$, where N is the number of molecules (or scatterers, depending on the application in mind) within a given volume (one resolution cell in the context of ultrasound imaging). See Destrempes and Cloutier⁶ for a list of references on applications in ultrasound backscattering of red blood cells. In the previous work,⁸ an empirical relation between the isotropic diameter of aggregates D and parameter $1/(\kappa + 1)$ was obtained on *in vitro* data. Although parameter D is empirically related¹⁴ to the packing factor W , it is nevertheless interesting to aim at a direct theoretical relation between W and parameter α .

^{a)}Electronic mail: francois.destrempes@crchum.qc.ca, ORCID: 0000-0002-2645-4196.

^{b)}Also at: Department of Radiology, Radio-Oncology and Nuclear Medicine, and Institute of Biomedical Engineering, University of Montreal, Montreal, Quebec, H3T 1J4, Canada.

To reach a physical interpretation of the statistical parameters of the echo envelope, one needs a generic model of the RF signals. In particular, a model for the point process of scatterers has to be considered. In Shankar,¹⁵ a derivation of the homodyned K-distribution was obtained (although this distribution was called a generalized K-distribution, which is not to be confused with the distribution bearing that name in Jakeman and Tough³) based on the assumption of independent scatterers. The same assumption was adopted in Chen *et al.*¹⁶ But as previous works^{12,17–19} have shown, this hypothesis is not valid, generally speaking. To address this difficulty, we had previously adopted^{4,8,9,20} the formalism of Jakeman *et al.*,^{2,3} where the scattering medium is viewed as a continuous medium that is discretized, yielding phasors related to local inhomogeneities in the scattering properties. In this work, we have considered directly the more general hypothesis of possibly correlated scatterers.

The main goal of this study was to develop the underlying theory to the preliminary results presented in Destrempes and Cloutier.⁶ For this purpose, we closely examined the generic model of RF signals by Chen *et al.*,²¹ which allowed the expression of the explicitly related phasors upon applying the strong law of large numbers, where each scatterer was randomly uniformly sampled, yielding sample (backscattering) points. We considered the stochastic process of the sample points in which the positions of scatterers and, hence, sample points, may be correlated. Inspired by the Jakeman and Tough³ model, which relies on a generalization of the central limit theorem, we considered Lyapounov's version of the central limit theorem²² in which the random variables are not necessarily identically distributed. This theorem was applied on partial sums of the phasors within small nonoverlapping cubes that cover one resolution cell. Inspired by Billingsley,²² the case in which the partial sums are dependent (whenever the scatterers are correlated) was addressed by comparing this process with the process in which the partial sums are (formally) independent through the Kolmogorov distance between these two processes. Furthermore, the latter (formal) process was compared to a normal distribution based on Lyapounov's constant²² and its relation to the Kolmogorov distance using an explicit version²³ of the Berry-Esseen theorem. The triangle inequality of the Kolmogorov distance then allowed us to assess the hypothesis of a normal distribution for the underlying stochastic physical process (before applying the absolute value) using the Kolmogorov-Smirnov goodness-of-fit test.²⁴ The implications on the Hilbert transform of the RF signals and their echo envelope was also developed. More generally, we considered a decomposition of the analytic signal into two components, denoted herein as X_φ and Y_φ , in such a way that the former component may be modeled with a 1D homodyned K-distribution and the latter may be modeled with a K-distribution. The numerical simulations showed that the hypothesis of a 1D homodyned K-distribution is viable for the absolute value of the RF signals and their Hilbert transform and, therefore, for the 2D homodyned K-distribution model of their echo envelope. The simulations were

performed with values of $\langle N \rangle$ and W , varying from 1 to 21 and 1 to 11, respectively.

This work is related to the inverse scattering theory. An overview of this field of research is presented in the review article of Colton and Kress.²⁵ In the special case of acoustical compressive waves and impenetrable scatterers (i.e., obstacles), one may consider the Helmholtz equation for the velocity potential with the sound-soft (homogeneous Dirichlet) boundary condition and Sommerfeld radiation condition.²⁵ Given an incident plane wave, one is interested in the scattered wave and its far field patterns at various observation and incident directions. One is then led to the inverse scattering problems, such as the existence of a solution and uniqueness of the obstacle knowing the far field patterns for given incident directions and at given wave numbers, assuming boundedness of the scatterer and connectivity and sufficient smoothness of its boundary. Several other inverse scattering problems have been investigated, including the sound-hard (homogeneous Neumann) boundary condition on obstacles, penetrable objects (i.e., inhomogeneities within a surrounding medium) for both isotropic and anisotropic materials.²⁵ Furthermore, inverse scattering problems have been considered in fields other than acoustics, notably in electromagnetism,^{26–29} mentioning only a few recent articles. Inverse scattering problems were also studied in the context of locally rough surfaces,³⁰ phaseless scattering data motivated by imaging of nanoscale structures and biological cells,³¹ elastic scattering with phaseless data,³² moving point source,³³ and deep learning approaches³⁴ to mention only a few recent works.

In this study, acoustically penetrable scatterers are implicitly considered [i.e., Eqs. (4.1)–(4.3) in Colton and Kress²⁵] as in Twersky,¹² i.e., an inhomogeneous medium, in this case, isotropic and absorbing. This framework is consistent with Eq. (8.1.14) in Morse and Ingard,³⁵ noticing that this reference treats the Helmholtz equation for the pressure field rather than the velocity potential as in Colton and Monk;³⁶ see Pierce.³⁷ The scatterers are viewed as the set of points (assumed to be a compact set) where the refractive index³⁶ differs from one as a result of a difference in the mass density and compressibility from the surrounding medium. Recall that the refractive index at a position \mathbf{r} is defined as the square of the ratio $c_0/c(\mathbf{r})$, where c_0 and $c(\mathbf{r})$ denote the speed of sound in the ambient medium and at position \mathbf{r} , respectively; it is assumed that $c(\mathbf{r}) = c_0$ for \mathbf{r} sufficiently large.³⁶ We have assumed the Born approximation under weak scattering, as in the work of Chen *et al.*²¹ in ultrasonics. The received signals in the far field are considered at several wave numbers, corresponding to the transducer's frequency bandwidth, combining several incident directions, according to the probe's design.

II. BACKGROUND ON ACOUSTICAL PHYSICS

A. Physical model of ultrasound signals

We adopt a convention that is consistent with previous works.^{21,35,38,39} The position of the observation point (i.e.,

the center of the transducer's surface) is herein denoted \mathbf{r}_0 . The position of the center of the scattering volume is denoted \mathbf{r} , whereas \mathbf{r}' represents the position of an arbitrary point within the scattering volume. Moreover, the unit direction vector of the incident wave is denoted $\hat{\mathbf{i}}$, whereas the lateral and elevation unit direction vectors are denoted $\hat{\mathbf{l}}$ and $\hat{\mathbf{e}}$, respectively. In this framework, the origin of the coordinate system can be fixed arbitrarily. But for the sake of simplicity, we take the origin of the coordinate system as the center of the transducer's surface (so, $\mathbf{r}_0 = \mathbf{0}$) and its axes to correspond with the unit vectors $\hat{\mathbf{l}}$, $\hat{\mathbf{e}}$, and $\hat{\mathbf{i}}$. With this convention, we will drop in the sequel any mention of \mathbf{r}_0 in the notation. See Fig. 1(a) for a schematic illustration of the notation.

We consider a homogeneous ambient medium with constant compressibility κ_0 (Pa^{-1}), mass density ρ_0 (Kg/m^3), and speed of sound c_0 . We let the scattering medium (including the scatterers and their ambient medium) have variable compressibility $\kappa(\mathbf{r})$ and variable mass density $\rho(\mathbf{r})$. The fractional variation in the compressibility and mass density³⁸ within the scattering volume are then defined as $\gamma_\kappa(\mathbf{r}) = \kappa(\mathbf{r})/\kappa_0 - 1$ and $\gamma_\rho(\mathbf{r}) = 1 - \rho_0/\rho(\mathbf{r})$, respectively. We set $\gamma(\mathbf{r}) = \gamma_\kappa(\mathbf{r}) - \gamma_\rho(\mathbf{r})$, herein called the fractional variation in tissue acoustic properties.

In the context of insonification of the tissues with a transducer whose active elements are larger than the acoustic wavelength λ , the incident pressure wave at the angular frequency ω is of the form of Eq. (2) in Chen *et al.*,²¹

$$\hat{P}_{\text{in}}(\mathbf{r}' | \omega) e^{-i\omega t} = P_0(\omega) D_T(\mathbf{r}' | \omega) e^{-i\omega t}, \quad (1)$$

where $P_0(\omega)$ denotes the characteristic pressure amplitude (Pa) at the transducer's surface and $D_T(\mathbf{r}' | \omega)$ is the radiation pattern (no units) at transmission. See, also, Eq. (8) in Ng *et al.*³⁹ We assume that the incident wave behaves as a

plane wave, $\nabla \hat{P}_{\text{in}}(\mathbf{r}' | \omega) \approx \hat{P}_{\text{in}}(\mathbf{r}' | \omega) (ik\hat{\mathbf{i}})$, where $k = \omega/c_0 = 2\pi/\lambda$ is the wave number.

To take into account the acoustic attenuation due to the absorption and scattering, one considers the total attenuation coefficient³⁸ at the depth $z_0 = |\hat{\mathbf{i}} \cdot \mathbf{r}|$ (cm). Notice that under linear dependency in the frequency of the total attenuation coefficient, one has $\alpha(\mathbf{r}, \omega) = \alpha_0(\mathbf{r})f$, where $\alpha_0(\mathbf{r})$ is the total attenuation coefficient slope (ACS; $\text{Np cm}^{-1} \text{MHz}^{-1}$) and $f = \omega/(2\pi)$ denotes the frequency (MHz). We assume that the observation point is far away from the scattering volume (far field assumption). Then, one has the following expression for the average pressure (Pa; i.e., total force per unit surface) exerted on the transducer's surface at the reception:

$$P_0(\omega) e^{-\alpha(\mathbf{r})\omega z_0/\pi} \frac{ik}{2|S|} \int_V D_R(\mathbf{r}' | \omega) \gamma(\mathbf{r}') D_T(\mathbf{r}' | \omega) d^3(\mathbf{r}'), \quad (2)$$

where $|S|$ is the area of the transducer's surface and $D_T(\mathbf{r}' | \omega)$ is the radiation pattern (no units) at reception. See Eq. (15) in Chen *et al.*,²¹ where the equation is presented without the attenuation coefficient. In the sequel, we denote as $D(\mathbf{r}' | \omega)$ the product $D_R(\mathbf{r}' | \omega) D_T(\mathbf{r}' | \omega)$.

The received RF signal $\text{RF}(\mathbf{r}, t)$ (V) is then equal to

$$\int_{-\infty}^{\infty} H(\omega) e^{-\alpha(\mathbf{r})\omega z_0/\pi} \frac{ik}{2|S|} \int_V D(\mathbf{r}' | \omega) \gamma(\mathbf{r}') d^3(\mathbf{r}') e^{-i\omega t} d\omega, \quad (3)$$

where $H(\omega) = P_0(\omega) T_R(\omega) B(\omega)$ (V s), $T_R(\omega)$ is the acoustoelectric transfer function (V/Pa) of the transducer's elements at reception, and $B(\omega)$ is a bandpass filter applied to the received electrical signal. Observe that this expression is valid after canceling the time-gain compensation (TGC).⁴⁰

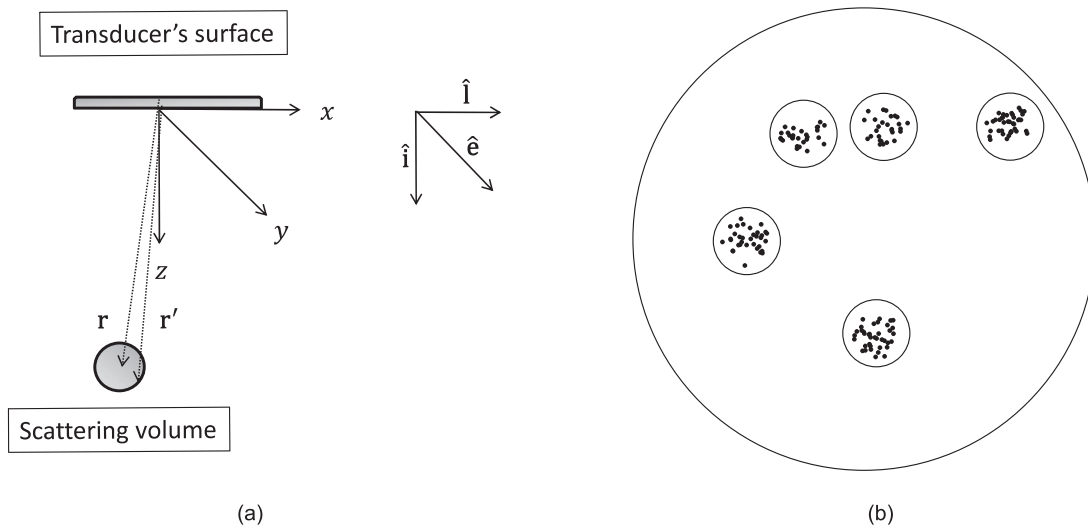


FIG. 1. (a) The coordinate system in use. The (x, y, z) -system has an origin located at the center of the transducer's surface and its axes are parallel to the unit vectors $(\hat{\mathbf{i}}, \hat{\mathbf{l}}, \hat{\mathbf{e}})$, which are defined with respect to the imaging plane—axial, lateral, and elevation directions, respectively. The vectors \mathbf{r} and \mathbf{r}' indicate the positions of the center of the scattering volume and an arbitrary point within the scattering volume, respectively. (b) The schematic illustration of the spherical scatterers within a scattering volume together with uniformly distributed sample points within each scatterer is shown.

Applying Fubini's theorem, one recasts Eq. (3) in the form

$$\int_V \int_{-\infty}^{\infty} H(\omega) e^{-\alpha(\mathbf{r})\omega z_0/\pi} \frac{ik}{2|S|} D(\mathbf{r}'|\omega) e^{-i\omega t} d\omega \gamma(\mathbf{r}') d^3(\mathbf{r}'). \quad (4)$$

Under the far field assumption, one may use the approximate form³⁹ of RF($\mathbf{r}, t = 2z/c_0$),

$$\int_V h(\mathbf{r}' - \mathbf{r}) \cos(2\tilde{k}_c(z' - z) + \varphi) \gamma(\mathbf{r}') d^3(\mathbf{r}'), \quad (5)$$

where $h(x, y, z)$ represents the effective point spread function (PSF) of the acoustic system and \tilde{k}_c is the nominal wave number, both of which take into account the downshifting resulting from the attenuation factor⁴¹ $e^{-\alpha(\mathbf{r})\omega z_0/\pi}$. Here, the angle φ is called the phase shift. The PSF is assumed to be proportional to a Gaussian-shaped function $e^{-x^2/2\tilde{\sigma}_x^2 - y^2/2\tilde{\sigma}_y^2 - z^2/2\tilde{\sigma}_z^2}$, where the lateral, elevation, and axial variances $\tilde{\sigma}_x^2$, $\tilde{\sigma}_y^2$, and $\tilde{\sigma}_z^2$, respectively, are expressed in the spatial domain. The value $\varphi = 0$ means that the transmitted pressure field (at the surface of the transducer) along the axial direction is of the form $p(t) \cos(\omega_c t)$, where $p(t)$ is a Gaussian-shaped function, and $\varphi = \pi/2$ means that it is of the form $p(t) \sin(\omega_c t)$.

We, thus, obtain the following expression for the (modulated) analytic complex signal $s(\mathbf{r}, t = 2z/c_0) = \text{RF}(\mathbf{r}, t = 2z/c_0) + i\mathcal{H}(\text{RF}(\mathbf{r}, t = 2z/c_0))$, where \mathcal{H} denotes Hilbert's transform, and its approximate form is

$$\begin{aligned} & \int_0^{\infty} H(\omega) e^{-\alpha(\mathbf{r})\omega z_0/\pi} \frac{ik}{|S|} \int_V D(\mathbf{r}'|\omega) \gamma(\mathbf{r}') d^3(\mathbf{r}') e^{-i\omega t} d\omega \\ & \approx \int_V h(\mathbf{r}' - \mathbf{r}) e^{2i\tilde{k}_c(z' - z) + i\varphi} \gamma(\mathbf{r}') d^3(\mathbf{r}'). \end{aligned} \quad (6)$$

This expression may be recast as

$$\begin{aligned} & \text{RF}(\mathbf{r}, t = 2z/c_0) + i\mathcal{H}(\text{RF}(\mathbf{r}, t = 2z/c_0)) \\ & = (X_\varphi(\mathbf{r}, t = 2z/c_0) + iY_\varphi(\mathbf{r}, t = 2z/c_0)) e^{i\varphi}, \end{aligned} \quad (7)$$

where $X_\varphi(\mathbf{r}, t = 2z/c_0)$ and $Y_\varphi(\mathbf{r}, t = 2z/c_0)$ are, therefore, approximated, respectively, as

$$\int_V h(\mathbf{r}' - \mathbf{r}) \cos(2\tilde{k}_c(z' - z)) \gamma(\mathbf{r}') d^3(\mathbf{r}'), \quad (8a)$$

$$\int_V h(\mathbf{r}' - \mathbf{r}) \sin(2\tilde{k}_c(z' - z)) \gamma(\mathbf{r}') d^3(\mathbf{r}'). \quad (8b)$$

To find out the phase shift φ , one may consider the response of the acquisition system to a wire located at the focal point and parallel to the elevation direction, i.e., Eq. (6) when a single scatterer is located at the focal position \mathbf{r}' . Then, summing up the analytic complex signal over a segment of length equal to the axial resolution and centered at the focal point yields a complex number of the form $e^{i\varphi}$ after normalization by its complex modulus. One can then compensate for this phase shift by multiplying the modulated

analytic signal with $e^{-i\varphi}$, which yields the complex signal $X_\varphi + iY_\varphi$ of Eq. (7). The real and imaginary parts of this resulting complex signal will then be of the form of Eqs. (8a) and (8b), respectively, in the case of the single scatterer. This property will then hold in the presence of an arbitrary configuration of scatterers.

B. Power spectrum of RF signals

The power spectrum $PS(\mathbf{r}, \omega)$ ($V^2 \text{ s}^2$) is defined as the average over the scanlines of the complex modulus squared of the Fourier transform of the received RF signals. Based on the cross-correlation theorem in Fourier analysis, one obtains the following approximate decomposition for the power spectrum in Chen *et al.*,²¹ Eqs. (18) and (19):

$$|H(\omega)|^2 e^{-2\alpha(\mathbf{r})\omega z_0/\pi} \text{BSC}(\mathbf{r}, k) \hat{D}(\mathbf{r}, \omega). \quad (9)$$

Here, the backscatter coefficient ($\text{m}^{-1} \text{ sr}^{-1}$) at position \mathbf{r} of the resolution cell is defined as an ensemble average [Eq. (7) in Insana *et al.*³⁸]

$$\text{BSC}(\mathbf{r}, k) = \frac{k^4}{16\pi^2 |V|} \left\langle \left| \int_V \gamma(\mathbf{r}') e^{2i\hat{\mathbf{k}} \cdot \mathbf{r}'} d^3(\mathbf{r}') \right|^2 \right\rangle, \quad (10)$$

where $|V|$ is the volume of one resolution cell at depth z_0 , and

$$\hat{D}(\mathbf{r}, \omega) = \left(\frac{2\pi}{k|S|} \right)^2 \int_V |D(\mathbf{r}'|\omega)|^2 d^3(\mathbf{r}') \quad (11)$$

is the diffraction factor (m sr) at position \mathbf{r} , which depends on beamforming [Eq. (18) in Chen *et al.*²¹] See Yu and Cloutier¹⁸ for a description of the structure factor size estimator (SFSE) model that relates the backscatter coefficient with the packing factor.

Let us mention that the ensemble average of the RF signal has a Fourier transform whose squared complex modulus $|\langle \widehat{\text{RF}}(\mathbf{r}, \omega) \rangle|^2$ is approximately equal to

$$|H(\omega)|^2 e^{-2\alpha(\mathbf{r})\omega z_0/\pi} \text{BSC}_{\text{coh}}(\mathbf{r}, k) \hat{D}(\mathbf{r}, \omega), \quad (12)$$

where the coherent backscatter coefficient $\text{BSC}_{\text{coh}}(\mathbf{r}, k)$ is defined as

$$\frac{k^4}{16\pi^2 |V|} \left| \int_V \langle \gamma(\mathbf{r}') e^{2i\hat{\mathbf{k}} \cdot \mathbf{r}'} \rangle d^3(\mathbf{r}') \right|^2. \quad (13)$$

See de Monchy *et al.*⁴² for further results on the coherent component of ultrasound signals.

III. THE RF SIGNALS VIEWED AS STOCHASTIC PROCESS

A. Assumptions

We now consider an ensemble of N scatterers, where N is viewed as a discrete random variable. We assume that the

positions of the scatterers are distributed according to a stochastic point process, possibly other than a homogeneous Poisson process, thus, allowing (statistical) dependency between the scatterers' random positions. Next, we sample within each scatterer (indexed with i) M_i random points, herein, called sample backscattering points or sample points for short, according to a homogeneous Poisson process (within each scatterer). We let the discrete variables M_i be independent Poisson variables with the same mean and variance equal to M_0 . We, therefore, obtain an overall ensemble of $N_0 = \sum_{i=1}^N M_i$ sample (backscattering) points, which are henceforth distributed according to a point process, possibly other than a homogeneous Poisson point process. See Fig. 1(b) for a schematic illustration of sample points within the spherical scatterers.

We denote $\mathbf{r}'_1, \mathbf{r}'_2, \dots, \mathbf{r}'_{N_0}$ as the positions of the sample points. We let $|V_n|$ denote the volume $|V_{s,i}|$ of a single scatterer divided by M_i (assuming that the n th sample point located at position \mathbf{r}'_n belongs to the i th scatterer). We set $\gamma_n = \gamma(\mathbf{r}'_n)$ and define $\alpha_n = |V_n|\gamma_n$. The factor $|V_n|$ arises from the (strong) law of large numbers, as explained briefly after Eq. (15), rather than a subdivision of each scatterer into M_i disjoint physical pieces.

Then, substituting the function $\alpha_n \delta(\mathbf{r}' - \mathbf{r}'_n)$ into Eq. (3), one obtains the random variable,

$$b_n = \alpha_n \int_{-\infty}^{\infty} H(\omega) e^{-\alpha(\mathbf{r})\omega z_0/\pi} \frac{ik}{2|S|} D(\mathbf{r}'_n | \omega) e^{-2ikz} d\omega, \quad (14)$$

where we used the change of variable $z = c_0 t/2$. Next, one has an approximation for the fractional variation in the tissue acoustic properties function,

$$\gamma(\mathbf{r}'_n) \approx \sum_{n=1}^{N_0} \alpha_n \delta(\mathbf{r}' - \mathbf{r}'_n). \quad (15)$$

This yields the following stochastic process for $\text{RF}(\mathbf{r}, t = 2z/c_0)$ and its approximation based on Eq. (5),

$$\sum_{n=1}^{N_0} b_n \approx \sum_{n=1}^{N_0} \alpha_n h(\mathbf{r}'_n - \mathbf{r}) \cos(2\tilde{k}_c(z'_n - z) + \varphi). \quad (16)$$

Notice that Eq. (16) follows from Eq. (3) by the strong law of large numbers because the sample points are uniformly distributed within each scatterer. Indeed, the inner integral $\int_V D(\mathbf{r}' | \omega) \gamma(\mathbf{r}') d^3(\mathbf{r}')$ in Eq. (3) may be expressed as the sum of the corresponding integrals over the volume covering each scatterer. For each term (corresponding to the i th scatterer), as $1 = |V_{s,i}| |V_{s,i}|^{-1}$ and $|V_{s,i}|^{-1}$ is the probability density function (PDF) of the uniform distribution on the scatterer, the law of large numbers allows replacing the term with the (random) average $|V_{s,i}|(1/M_i) \sum_{\nu=1}^{M_i} D(\mathbf{r}'_{n_\nu} | \omega) \gamma(\mathbf{r}'_{n_\nu})$, where \mathbf{r}'_{n_ν} , $\nu = 1, \dots, M_i$, are the positions of the sample points within the scatterer.

Because the scatterers within one resolution cell contribute most to the received signals at a given position \mathbf{r} , we

may assume that N_0 represents the total number of sample (backscattering) points within the resolution cell centered at \mathbf{r} . Note that we found it more convenient in the proposed theoretical framework to sample points within each scatterer rather than sampling points over the entire scattering volume, in which case, some of the points would fall into the ambient medium rather than within the scatterers.

B. Interpretation of parameter α

Under the above hypotheses on the discrete random variables N and M_i , $i = 1, \dots, N$, the average number of sample backscattering points is equal to $\langle N_0 \rangle = \langle N \rangle M_0$. Observe that conditional to N , N_0 is a Poisson distribution of mean and variance equal to $N M_0$. Furthermore, based on the notion of the packing factor^{12,13} W , one has $\text{Var}[N] = W \langle N \rangle$, where $\langle N \rangle$ is the average number of scatterers within one resolution cell.

We now show that the variance of N_0 is asymptotic to $W \langle N \rangle M_0^2$ and N_0 may be modeled with a negative binomial distribution $N\text{Bin}(\alpha, p)$, defined as in Jakeman and Tough,³ for which the parameter α is equal to

$$\alpha = \frac{\langle N \rangle}{W}. \quad (17)$$

Under the above assumptions, the average number of sample points is equal to $\langle N_0 \rangle = \langle \sum_{i=1}^N M_i \rangle = \langle N \rangle M_0$. Moreover, one may compute the variance of the number of sample points, where $M_0 \gg 0$, as

$$\begin{aligned} \text{Var}[N_0] &= \left\langle \left(\sum_{i=1}^N M_i \right)^2 \right\rangle - \langle N \rangle^2 M_0^2 \\ &\sim (\langle N \rangle + \langle N(N-1) \rangle - \langle N \rangle^2) M_0^2 = W \langle N \rangle M_0^2. \end{aligned} \quad (18)$$

Now, from Eq. (54) in Frank and Smith,⁴³ the discrete distribution with maximal entropy (viewed as the most probable distribution) among the ones with mean $\langle N \rangle M_0$ and variance $W \langle N \rangle M_0^2$ is the negative binomial distribution defined as in Destempes and Cloutier,⁹

$$N\text{Bin}(N_0 | \alpha, p) = \frac{\Gamma(N_0 + \alpha)}{N_0! \Gamma(\alpha)} (1-p)^{N_0} p^\alpha. \quad (19)$$

Notice that Eq. (54) in Frank and Smith⁴³ may be applied as long as $\text{Var}[N_0] > \langle N_0 \rangle$, i.e., whenever $W M_0 > 1$, which holds for $M_0 \gg 0$ given any $W > 0$. Furthermore, in Eq. (19), one has the limit values

$$p = \frac{\langle N_0 \rangle}{\text{Var}[N_0]} = \frac{\langle N \rangle M_0}{W \langle N \rangle M_0^2} \xrightarrow{M_0 \rightarrow \infty} 0, \quad (20a)$$

$$\alpha = \frac{1 - \langle N_0 \rangle^2}{(1-p) \text{Var}[N_0]} = \frac{1 - \langle N \rangle^2 M_0^2}{(1-p) W \langle N \rangle M_0^2} \xrightarrow{M_0 \rightarrow \infty} \frac{\langle N \rangle}{W}, \quad (20b)$$

where we have used Secs. 2.1.3 and 8.7.1 in Rice.⁴⁴ Note that $N\text{Bin}(N_0 = 0 | \alpha, p) = p^\alpha$, which converges to zero as M_0 tends to infinity.

An important issue is then to settle what is exactly meant by the (effective) resolution cell. This issue will be discussed below.

C. Central limit theorem for the RF signals

We set $a_n = b_n - \langle b_n \rangle$ and we introduce the random variables $B_n = M_0 b_n$ and $A_n = B_n - \langle B_n \rangle = M_0 a_n$. We consider the following parameters (see step 2 below):

$$\bar{\mu} = \langle N \rangle \langle B_1 \rangle; \quad \bar{\tau}^2 = \langle N \rangle^2 \langle A_1 A_2 \rangle. \tag{21}$$

We now show that conditional to N , and for large values of M_0 , the random variable $b = \sum_{n=1}^{N_0} b_n$ has a PDF that may be approximated with a 1D normal distribution,

$$\mathcal{N}(b | \bar{\mu}, (N/\langle N \rangle)\bar{\tau}^2). \tag{22}$$

It follows that its absolute value $X = |\sum_{n=1}^{N_0} b_n|$ has a PDF that may be modeled with a 1D Rice distribution [see Eq. (4) with $n = 1$ in Destrempes and Cloutier⁹]

$$P_{\text{Rice},d=1}(X | |\bar{\mu}|, (N/\langle N \rangle)\bar{\tau}^2). \tag{23}$$

For this purpose, we consider N_0 sample backscattering points within a scattering volume V , which encompasses one resolution cell. We consider the random variables $b_n, n = 1, \dots, N_0$, appearing in Eq. (16). We assume, as in Sec. III A, that $N_0 = \sum_{i=1}^N M_i$, where N is the number of scatterers and M_i is the number of sample points within the i th scatterer and M_i is a discrete Poisson variable with mean (and hence, variance) equal to M_0 . It follows that conditional to N , the variable N_0 is a Poisson variable of mean equal to NM_0 . We let $\langle N \rangle$ denote the average number of scatterers (per resolution cell).

Step 1. We partition a rectangular box R circumscribing V into M disjoint cubes $C_m (m = 1, \dots, M)$ of the same dimensions. We assume that each cube contains N_m sample backscattering points such that $N_0 = \sum_{m=1}^M N_m$. We set

$$U_m = \sum_{\mathbf{r}_n \in C_m} b_n - \left\langle \sum_{\mathbf{r}_n \in C_m} b_n \right\rangle, \tag{24}$$

where the average is over all realizations of the point process, thus, allowing the variables M_i to fluctuate, but conditional to a fixed number of scatterers N . We then define the random variable

$$U = \sum_{n=1}^{N_0} b_n - \left\langle \sum_{n=1}^{N_0} b_n \right\rangle = \sum_{m=1}^M U_m. \tag{25}$$

By definition, one has $\langle U_m \rangle = 0$. We assume that the random variables U_m are almost mutually independent (in a sense, which is made precise below). This assumption seems reasonable provided that the correlation length between the sample backscattering points is smaller than the diameter of

the cubes whilst ignoring the boundary conditions for the adjacent cubes.

For this purpose, we consider M independent variables U'_m , for $m = 1, \dots, M$, each one distributed as U_m . We then define the random variable

$$U' = \sum_{m=1}^M U'_m. \tag{26}$$

In view of Lyapounov's theorem (Theorem 27.3 in Billingsley²²), we wish to verify Lyapounov's condition [Eq. (27.16) in Billingsley²²]. We define

$$s^2 = \sum_{m=1}^M E[|U'_m|^2], \tag{27}$$

where $E[\cdot]$ denotes the ensemble averaging operator $\langle \cdot \rangle$ in this context. We consider for $\delta > 0$ Lyapounov's constant, defined as

$$L_{M,\delta} = \sum_{m=1}^M \frac{E[|U'_m|^{2+\delta}]}{s^{2+\delta}}. \tag{28}$$

To demonstrate that the random variable U'/s is close to the standard normal variable $\mathcal{N}(0, 1)$, the proposed strategy is to provide an estimate for Lyapounov's constant in Eq. (28) in the case where $\delta = 1$ and then resort to a sharp version²³ of the Berry-Esseen theorem for a bound on the Kolmogorov distance between these two random variables. Provided $L_{M,1}$ is small, one may then conclude that U'/s is close to the standard normal variable $\mathcal{N}(0, 1)$. Henceforth, provided $U/\sqrt{\text{Var}[U]}$ and U'/s are close distributions, we may conclude that $U/\sqrt{\text{Var}[U]}$ is close to the standard normal variable $\mathcal{N}(0, 1)$.

Step 2. We compute, conditional to N ,

$$\left\langle \sum_{n=1}^{N_0} b_n \right\rangle = NM_0 \langle b_1 \rangle = \mu, \tag{29a}$$

$$\begin{aligned} \text{Var}[U] &= \left\langle \left(\sum_{n=1}^{N_0} b_n - \left\langle \sum_{n=1}^{N_0} b_n \right\rangle \right)^2 \right\rangle \\ &\sim (NM_0)^2 (\langle b_1 b_2 \rangle - \langle b_1 \rangle^2) = \tau^2, \end{aligned} \tag{29b}$$

where we are taking large values of M_0 . We also consider the following parameters:

$$\bar{\mu} = \langle N \rangle M_0 \langle b_1 \rangle, \tag{30a}$$

$$\bar{\tau}^2 = (\langle N \rangle M_0)^2 \langle a_1 a_2 \rangle. \tag{30b}$$

We notice that, on average, over all of the values of N , the differences between μ and $\bar{\mu}$, and between τ^2 and $\nu\bar{\tau}^2$, where $\nu = N/\langle N \rangle$, are equal to zero. Thus, we content that μ and τ^2 may be replaced with $\bar{\mu}$ and $\nu\bar{\tau}^2$, respectively. Consider that the average difference between τ^2 and $\bar{\tau}^2$ is equal to $W\langle N \rangle (M_0)^2 \langle a_1 a_2 \rangle$, which certainly cannot be ignored. We notice that Eqs. (30a) and (30b) amount to the two expressions in Eq. (21) based on the following two lemmas.

Lemma 1: The negative binomial distribution $NBin(N_0 | \alpha, p)$ may be viewed as the compound Poisson-gamma distribution,

$$\int_0^\infty \text{Poisson}(N_0 | M_0 \lambda) \mathcal{G}(\lambda | \alpha, W) d\lambda \quad (31a)$$

$$= \int_0^\infty \text{Poisson}(N_0 | \langle N \rangle M_0 \nu) \mathcal{G}(\nu | \alpha, 1/\alpha) d\nu. \quad (31b)$$

Proof: From Ref. 45 one has the Poisson-gamma compound representation,

$$NBin(N_0 | \alpha, p) = \int_0^\infty \text{Poisson}(N_0 | \lambda) \mathcal{G}(\lambda | \alpha, (1-p)/p) d\lambda. \quad (32)$$

With the change of variable $\lambda = M_0 \lambda'$, the right-hand side of this expression is equivalent to

$$\int_0^\infty \text{Poisson}(N_0 | M_0 \lambda') \mathcal{G}(M_0 \lambda' | \alpha, (1-p)/p) M_0 d\lambda'. \quad (33)$$

But, one has $\mathcal{G}(M_0 \lambda' | \alpha, (1-p)/p) M_0 = \mathcal{G}(\lambda' | \alpha, (1-p)/(M_0 p))$ and $\lim_{M_0 \rightarrow \infty} (1-p)/M_0 p = \langle N \rangle / \alpha = W$. We, thus, obtain Eq. (31a). The change of variable $\lambda = \langle N \rangle \nu$ then yields Eq. (31b).

Therefore, in Eq. (31a), the random variable λ represents the number N of scatterers within one resolution cell (not to be confused with the wavelength), whereas M_0 is the average number of sample points per scatterer. Henceforth, in Eq. (31b), the random variable ν represents $N/\langle N \rangle$.

Lemma 2: Given the Poisson distribution with mean λ , one has $\lim_{\lambda \rightarrow \infty} \text{Poisson}(n | \lambda) = 0$. Moreover, one has $\sum_{n=1}^\infty n^{-1} \text{Poisson}(n | \lambda) \sim 1/\lambda$, as λ tends to infinity.

Proof: For the first statement, notice that by definition, one has $\text{Poisson}(n = 0 | \lambda) = e^{-\lambda}$. For the second statement, we define the function $f(\lambda) = \sum_{n=1}^\infty n^{-1} \text{Poisson}(n | \lambda)$ and observe that this function satisfies the following linear differential equation with constant coefficients $f(\lambda) + f'(\lambda) = (1 - e^{-\lambda})/\lambda$. Indeed, performing term by term differentiation, one obtains

$$f'(\lambda) = \frac{1}{\lambda} \sum_{n=1}^\infty \frac{\lambda^n}{n!} e^{-\lambda} - f(\lambda). \quad (34)$$

The general solution is of the form $f(\lambda) = c(\lambda)e^{-\lambda}$, where $c(\lambda) = \int (e^\lambda - 1)/\lambda d\lambda$. With the help of the software Mathematica (Wolfram Research, Inc., Champaign, IL, version 11.3), we obtained the solution $f(\lambda) = (c_0 + Ei(\lambda) - \log \lambda)e^{-\lambda}$ for some constant c_0 , where Ei denotes the exponential integral function, i.e., the principal value of the integral $-\int_{-\lambda}^\infty e^{-t}/tdt$. Also, with the help of the software Mathematica, we computed

$$\lim_{\lambda \rightarrow \infty} \frac{(c_0 + Ei(\lambda) - \log \lambda)e^{-\lambda}}{1/\lambda} = 1. \quad (35)$$

Step 3. To realize the above strategy proposed in step 1, we first compute the Kolmogorov distance $\rho(F, F')$

$= \sup_x |F(x) - F'(x)|$, where $F(x)$ and $F'(x)$ are the cumulative functions of the random variables U/τ and U'/s , respectively. We assume an estimate

$$\rho(F, F') \approx \epsilon. \quad (36)$$

Note that an estimate can be obtained from two samples of the variables U and U' by using the empirical variance on the samples for $\tau = \text{Var}[U]$ and $s = \text{Var}[U']$. Next, we consider an estimate of Lyapounov's constant,

$$L_{M,1} = \frac{\sum_{m=1}^M E[|U'_m|^3]}{\left(\sum_{m=1}^M E[|U'_m|^2]\right)^{3/2}} \approx L_1. \quad (37)$$

Such an estimate can be obtained from a sample of the variables U'_m used to compute U' .

Step 4. We now deduce the theoretical consequences of conditions (36) and (37).

Theorem 1. Assume that condition (37) holds. Then, one has

$$\rho(F', \Phi) \leq C_0 L_1, \quad (38)$$

where $\rho(F', \Phi) = \sup_x |F'(x) - \Phi(x)|$ is the Kolmogorov distance between the cumulative functions $F'(x)$ and $\Phi(x) = 1/\sqrt{2\pi} \int_{-\infty}^x e^{-u^2/2} du$ of the random variables U'/s and $\mathcal{N}(0, 1)$, respectively. Here, C_0 is an absolute constant known to be less than 0.5583.

Proof: This follows directly from the Berry-Esseen theorem and the estimate of C_0 appearing in Ref. 23.

Corollary 1: Assume conditions (36) and (37) hold. Then, one has an upper bound

$$\rho(F, \Phi) \leq \epsilon + C_0 L_1. \quad (39)$$

Proof: Inequality (39) follows directly from condition (36) and Theorem 1 using the fact that the Kolmogorov distance satisfies the triangle inequality.

D. Distribution of the absolute value of the RF signals

Summing up over all of the values of the discrete random variable N , we, thus, obtain the distribution

$$\sum_{N=1}^\infty P_{\text{Rice},d=1}(X | |\bar{\mu}|, (N/\langle N \rangle)\bar{\tau}^2) \text{Prob}(N/\langle N \rangle), \quad (40)$$

which may be approximated with

$$\int_0^\infty P_{\text{Rice},d=1}(X | |\bar{\mu}|, \nu\bar{\tau}^2) \mathcal{G}(w | \alpha, 1/\alpha) d\nu, \quad (41)$$

where we used Lemma 1 and $\mathcal{G}(w | \alpha, \theta)$ denotes the gamma distribution with the shape parameter α and scale parameter θ . After the change of variable $w = \alpha\nu$, one obtains

$$\int_0^\infty P_{\text{Rice},d=1}(X | |\bar{\mu}|, (w/\alpha)\bar{\tau}^2)\mathcal{G}(w | \alpha, 1)dw. \quad (42)$$

But, because $\alpha = \langle N \rangle / W$, one has $\bar{\tau}^2 / \alpha = W \langle N \rangle \langle A_1 A_2 \rangle$. Moreover, one has $|\bar{\mu}| = \langle N \rangle \langle B_1 \rangle$. We, therefore, obtain the following compound distribution:

$$\int_{w=0}^\infty P_{\text{Rice},d=1}(X | \varepsilon_{\text{RF}}, \sigma_{\text{RF}}^2)\mathcal{G}(w | \alpha, 1)dw, \quad (43)$$

where we set

$$\varepsilon_{\text{RF}} = \langle N \rangle \langle B_1 \rangle; \quad \sigma_{\text{RF}}^2 = W \langle N \rangle \langle A_1 A_2 \rangle. \quad (44)$$

Equation (44) turns out to represent the homodyned K-distribution of dimension one with parameters ε_{RF} , σ_{RF}^2 , and α [Eq. (13) with $n = 1$ in Destremes and Cloutier⁹] for the absolute value of the RF signal,

$$|\text{RF}(\mathbf{r}, t = 2z/c_0)| \sim P_{\text{HK},d=1}(X | \varepsilon_{\text{RF}}, \sigma_{\text{RF}}^2, \alpha). \quad (45)$$

Considering the absolute value of the Hilbert transform $\mathcal{H}(\text{RF})$ of the RF signal, one obtains, for the same reasons, a homodyned K-distribution of dimension one. The same argument applies to both signals X_φ and Y_φ appearing in Eqs. (8a) and (8b) (taking into account the form of the transmitted pressure field). In particular, one has the following distribution for the absolute value of the component X_φ :

$$|X_\varphi(\mathbf{r}, t = 2z/c_0)| \sim P_{\text{HK},d=1}(X | \varepsilon_{X_\varphi}, \sigma_{X_\varphi}^2, \alpha). \quad (46)$$

We now show that $\varepsilon_{Y_\varphi} = 0$. Substituting $\gamma(\mathbf{r}') \approx \alpha_n \delta(\mathbf{r}' - \mathbf{r}'_n)$, where $\alpha_n = |V_n| \gamma_n$, into Eq. (8b) yields the approximation $b_n \approx \alpha_n P(\mathbf{r}'_n - \mathbf{r}) \sin(2\tilde{k}_c(z'_n - z))$ for the component Y_φ . Furthermore, assuming the symmetry of the PSF with respect to the plane through the point located at position \mathbf{r} that is normal to the incident wave direction, one obtains $\langle b_n \rangle \approx \langle \alpha_n P(\mathbf{r}'_n - \mathbf{r}) \sin(2\tilde{k}_c(z'_n - z)) \rangle = 0$. It follows that $\varepsilon_{Y_\varphi} = \lim_{M_0 \rightarrow \infty} \langle N \rangle M_0 \langle b_n \rangle = 0$.

Thus, the absolute value of the component Y_φ of the analytic signal is actually distributed according to a K-distribution of dimension one [Eq. (8) with $n = 1$ in Destremes and Cloutier⁹]

$$|Y_\varphi(\mathbf{r}, \mathbf{r}_0, t = 2z/c_0)| \sim P_{\text{K},d=1}(Y | \sigma_{Y_\varphi}^2, \alpha). \quad (47)$$

As 1D homodyned K-distributions are involved in this context, one obtains the mean intensity values $\mu_{X_\varphi} = \varepsilon_{X_\varphi}^2 + \sigma_{X_\varphi}^2 \alpha$ and $\mu_{Y_\varphi} = \sigma_{Y_\varphi}^2 \alpha$ (Theorem 4 with $n = 1$ in Destremes and Cloutier⁹).

IV. THE ANALYTIC COMPLEX SIGNAL AND ITS ENVELOPE VIEWED AS STOCHASTIC PROCESSES

A. Assumptions

For the reasons explained in Sec. II A, we find it convenient to perform demodulation around the nominal center frequency \tilde{f}_c . This choice is innocuous because the echo

envelope does not depend on demodulation. Similar to Eq. (14), we consider the random vector corresponding to a single scatterer located at position \mathbf{r}'_n ,

$$\mathbf{b}_n \approx 2\alpha_n \int_0^\infty H(\omega) e^{-\alpha(\mathbf{r})\omega z_0/\pi} \frac{ik}{2|S|} D(\mathbf{r}'_n | \omega) e^{-2i(k-\bar{k})z} d\omega. \quad (48)$$

Based on the tissue function approximation equation (15), this yields the stochastic process for $s(\mathbf{r}, t = 2z/c_0) e^{2i\tilde{k}_c z}$,

$$\sum_{n=1}^{N_0} \mathbf{b}_n \approx \sum_{n=1}^{N_0} \alpha_n h(\mathbf{r}'_n - \mathbf{r}) e^{2i\tilde{k}_c z'_n + i\varphi}. \quad (49)$$

We introduce the random variables $\mathbf{a}_n = \mathbf{b}_n - \langle \mathbf{b}_n \rangle$, $\mathbf{B}_n = M_0 \mathbf{b}_n$, and $\mathbf{A}_n = \mathbf{B}_n - \langle \mathbf{B}_n \rangle = M_0 \mathbf{a}_n$. We consider the following parameters:

$$\bar{\mu} = \langle N \rangle \langle B_1 \rangle; \quad \bar{\tau}^2 = \frac{1}{2} \langle N \rangle^2 \langle A_1 \bar{A}_2 \rangle. \quad (50)$$

B. Demodulated analytic signal

It is shown in this subsection that conditional to N , $\sum_{n=1}^{N_0} \mathbf{b}_n - \langle \sum_{n=1}^{N_0} \mathbf{b}_n \rangle$ can be viewed as a random vector with uncorrelated real and imaginary parts with the same variance.

Substituting $\gamma(\mathbf{r}') \approx \alpha_n \delta(\mathbf{r}' - \mathbf{r}'_n)$, where $\alpha_n = |V_n| \gamma_n$, into Eq. (6) yields after demodulation around the nominal center frequency,

$$\mathbf{b}_n \approx \left(\alpha_n h(\mathbf{r}'_n - \mathbf{r}) e^{2i\tilde{k}_c(z'_n - z) + i\varphi} \right) e^{2i\tilde{k}_c z}, \quad (51)$$

where h denotes the PSF and φ represents the phase shift as explained in Sec. II A. The random vector $\mathbf{a} = \sum_{n=1}^{N_0} \mathbf{b}_n - \langle \sum_{n=1}^{N_0} \mathbf{b}_n \rangle$ may, thus, be recast in the form

$$(A + iB)(\cos(2\tilde{k}_c z) + i \sin(2\tilde{k}_c z)), \quad (52)$$

where the two factors are viewed as independent random variables, the former depending only on the scatterers' acoustical properties and their relative positions to the geometric center of a resolution cell, whereas the latter depends only on the position of the resolution cell's geometric center. Given a function $f(z)$ of the axial coordinate z , we let $E_{\text{loc},z}[f(z)]$ denote its average along the axial direction over an interval centered at z of length equal to an effective axial resolution $\tilde{\ell}_z$ (described explicitly below). With the convention that $E[w] = E_{\text{loc},z}[\langle w \rangle]$, one then computes $E[|\text{Re}(\mathbf{a})|^2]$ as

$$\begin{aligned} & \langle A^2 \rangle E_{\text{loc},z}[\cos^2(2\tilde{k}_c z)] + \langle B^2 \rangle E_{\text{loc},z}[\sin^2(2\tilde{k}_c z)] \\ & - 2\langle AB \rangle E_{\text{loc},z}[\cos(2\tilde{k}_c z) \sin(2\tilde{k}_c z)]. \end{aligned} \quad (53)$$

This simplifies to $(\langle A^2 \rangle + \langle B^2 \rangle)(n/2)$, provided that the effective axial resolution $\tilde{\ell}_z$ is taken of the form $(n/2)\tilde{\lambda}_c$,

where n denotes a positive integer, since $2\tilde{k}_c(n/2)\tilde{\lambda}_c = 2\pi n$. Similarly, one computes $E[|\text{Im}(\mathbf{a})|^2]$ as

$$\begin{aligned} \langle A^2 \rangle E_{\text{loc},z}[\sin^2(2\tilde{k}_c z)] + \langle B^2 \rangle E_{\text{loc},z}[\cos^2(2\tilde{k}_c z)] \\ + 2\langle AB \rangle E_{\text{loc},z}[\sin(2\tilde{k}_c z) \cos(2\tilde{k}_c z)], \end{aligned} \quad (54)$$

which is equal to $E[|\text{Re}(\mathbf{a})|^2]$ under the same assumptions. Last, one may compute $E[\text{Re}(\mathbf{a})\text{Im}(\mathbf{a})]$:

$$-\langle AB \rangle E_{\text{loc},z}[\sin^2(2\tilde{k}_c z)] + \langle AB \rangle E_{\text{loc},z}[\cos^2(2\tilde{k}_c z)], \quad (55)$$

which cancels out to zero under the above assumptions.

C. Effective resolution cell

From the argument presented in Sec. IV B, one needs $(n/2)\tilde{\lambda}_c \geq \ell_z$, where $\tilde{\lambda}_c$ is the effective wavelength, i.e., depending on the total attenuation and the scanner's settings. Hence, ℓ_z is replaced with an effective axial resolution,

$$\tilde{\ell}_z = \frac{n}{2}\tilde{\lambda}_c; \quad n = \lceil 2\ell_z/\tilde{\lambda}_c \rceil. \quad (56)$$

In the lateral and elevation directions, we consider the actual resolutions ℓ_x and ℓ_y , respectively.

Based on a Gaussian-shaped PSF $h(x, y, z)$, i.e., proportional to $e^{-x^2/2\sigma_x^2 - y^2/2\sigma_y^2 - z^2/2\sigma_z^2}$, the surface of the effective resolution cell at -20 dB is the ellipsoid with the equation $2(x^2/2\sigma_x^2 + y^2/2\sigma_y^2 + z^2/2\sigma_z^2) = \log 100$. One, thus, obtains the resolutions $\ell_x/2 = \sqrt{\log 100}\sigma_x$, $\ell_y/2 = \sqrt{\log 100}\sigma_y$, and $\tilde{\ell}_z/2 = \sqrt{\log 100}\sigma_z$. The volume of one effective resolution cell is then equal to $|\tilde{V}| = (\tilde{\ell}_z/\ell_z) \times |V|$, where $|V|$ is the volume of the resolution cell itself.

Furthermore, to be consistent with Eq. (7) in Chen *et al.*,¹⁶ in the case of a single scatterer per unit volume, one would obtain $\alpha \approx 2(\iint\iint h^2(x, y, z) dx dy dz)^2 / \iint\iint h^4(x, y, z) dx dy dz$, which is equal to $2\sqrt{2}\pi\sigma_x\sqrt{2}\pi\sigma_y\sqrt{2}\pi\sigma_z$, whereas $|\tilde{V}| = (4\pi/3)(\sqrt{\log 100})^3\sigma_x\sigma_y\sigma_z$. Because $2(2\pi)^{3/2}/(4/3)\pi(\log 100)^{3/2} \approx 0.7609$, one obtains the interpretation

$$\alpha \approx 0.7609 \times \frac{m\tilde{V}}{W} = \left(0.7609 \times \frac{\tilde{\ell}_z}{\ell_z}\right) \times \frac{m|V|}{W}, \quad (57)$$

which amounts to a volume $\hat{V} = 0.7609 \times \tilde{V}$.

D. Central limit theorem for the analytic signal

It is now shown that the stochastic process $\sum_{n=1}^{N_0} \mathbf{b}_n$ conditional to N may be modeled with a Gaussian distribution of mean $\bar{\boldsymbol{\mu}}$ and isotropic variance with both components equal to $(N/\langle N \rangle)\bar{\tau}^2$,

$$\mathcal{N}(\mathbf{b} | \bar{\boldsymbol{\mu}}, (N/\langle N \rangle)\bar{\tau}^2 I_{2 \times 2}), \quad (58)$$

where $I_{2 \times 2}$ denotes the 2×2 identity matrix.

Conditional to N , one has

$$\left\langle \sum_{n=1}^{N_0} \mathbf{b}_n \right\rangle \approx NM_0 \langle \mathbf{b}_1 \rangle = \boldsymbol{\mu}. \quad (59)$$

Next, based on Eqs. (53)–(55), the diagonal components of the isotropic variance matrix $\text{Var}[\mathbf{a}]$, where $\mathbf{a} = \sum_{n=1}^{N_0} \mathbf{b}_n - \langle \sum_{n=1}^{N_0} \mathbf{b}_n \rangle$, are each equal to $\tau^2 = \frac{1}{2} E_{\text{loc},z}[\langle |\mathbf{a}|^2 \rangle]$, which in turn is equal to $\frac{1}{2} \langle |\mathbf{a}|^2 \rangle$ because the complex modulus of $e^{2i\tilde{k}_c z}$ is equal to one. By the stationarity of the point process of the sample backscattering points, for large values of M_0 and conditional to N , one computes

$$\begin{aligned} \frac{1}{2} \langle |\mathbf{a}|^2 \rangle &= \frac{1}{2} \left\langle \left| \sum_{n=1}^{N_0} \mathbf{b}_n - \left\langle \sum_{n=1}^{N_0} \mathbf{b}_n \right\rangle \right|^2 \right\rangle \\ &\sim \frac{1}{2} (NM_0)^2 \langle \mathbf{a}_1 \bar{\mathbf{a}}_2 \rangle = \tau^2. \end{aligned} \quad (60)$$

Similar to step 2 of Sec. III C, we consider the following parameters:

$$\bar{\boldsymbol{\mu}} = \langle N \rangle M_0 \langle \mathbf{b}_1 \rangle; \quad \bar{\tau}^2 = \frac{1}{2} (\langle N \rangle M_0)^2 \langle \mathbf{a}_1 \bar{\mathbf{a}}_2 \rangle. \quad (61)$$

We observe that, on average, over all of the values of N , the differences between $\boldsymbol{\mu}$ and $\bar{\boldsymbol{\mu}}$ and τ^2 and $\nu\bar{\tau}^2$, where $\nu = N/\langle N \rangle$, are equal to zero. Thus, we are replacing $\boldsymbol{\mu}$ and τ^2 with $\bar{\boldsymbol{\mu}}$ and $\nu\bar{\tau}^2$, respectively. We notice that the expressions in Eq. (61) amount to the two expressions in Eq. (50) based on Lemma 2. It remains to show that both real and imaginary parts of \mathbf{a} are close to a Gaussian distribution with the mean and variance equal to zero and τ^2 , respectively. But this hypothesis is reasonable for the reasons explained in Sec. III C.

E. Echo envelope distribution

From Eq. (6), one deduces the following approximation:

$$\left\langle \sum_{n=1}^{N_0} \mathbf{b}_n \right\rangle \approx \langle N_0 \rangle \langle \alpha_n h(\mathbf{r}'_n - \mathbf{r}) e^{2i\tilde{k}_c(z'_n - z) + i\phi} \rangle e^{2i\tilde{k}_c z}, \quad (62)$$

where $\alpha_n = |V_n| \gamma_n$. It follows that $\langle \sum_{n=1}^{N_0} \mathbf{b}_n \rangle$ has a constant amplitude and random phase equal to $2\tilde{k}_c z$, which is uniformly distributed. From there it follows that the complex modulus of the right-hand side of Eq. (49), $A = |\sum_{n=1}^{N_0} \mathbf{b}_n|$, may be modeled with a 2D Rice distribution [Eq. (4) with $n = 2$ in Destremes and Cloutier⁹]

$$P_{\text{Rice},d=2}(A | |\bar{\boldsymbol{\mu}}|, (N/\langle N \rangle)\bar{\tau}^2). \quad (63)$$

Summing up over all of the values of the discrete variable N , we, hence, obtain the distribution

$$\sum_{N=1}^{\infty} P_{\text{Rice},d=2}(A | |\bar{\boldsymbol{\mu}}|, (N/\langle N \rangle)\bar{\tau}^2) \text{Prob}(N/\langle N \rangle). \quad (64)$$

This distribution may be approximated with the compound distribution,

$$\int_0^\infty P_{\text{Rice},d=2}(A | \varepsilon, \sigma^2 w) \mathcal{G}(w | \alpha, 1) dw, \quad (65)$$

where we set

$$\varepsilon = \langle N \rangle |\langle \mathbf{B}_1 \rangle|; \quad \sigma^2 = \frac{1}{2} W \langle N \rangle \langle \mathbf{A}_1 \bar{\mathbf{A}}_2 \rangle. \quad (66)$$

This is the 2D homodyned K-distribution [Eq. (13) with $n = 2$ in Destrempes and Cloutier⁹]

$$|s(r, t = 2z/c_0)| \sim P_{\text{HK},d=2}(A | \varepsilon, \sigma^2, \alpha), \quad (67)$$

with parameters $\varepsilon, \mu = \varepsilon^2 + 2\sigma^2\alpha$.

Notice that the three distributions in Eqs. (46), (47), and (67) share the same parameter α , given by Eq. (17).

It is now shown that $\mu = \mu_{X_\varphi} + \mu_{Y_\varphi}$, $\varepsilon^2 = \varepsilon_{X_\varphi}^2$, and $\sigma^2 = (\sigma_{X_\varphi}^2 + \sigma_{Y_\varphi}^2)/2$. From Eq. (7) and because $|e^{i\varphi}| = 1$, one obtains

$$\langle |s(r, r_0, t)|^2 \rangle = \langle |X_\varphi(\mathbf{r}, \mathbf{r}_0, t)|^2 \rangle + \langle |Y_\varphi(\mathbf{r}, \mathbf{r}_0, t)|^2 \rangle, \quad (68)$$

which proves the first identity. Furthermore, one obtains the relation

$$\langle |s(r, r_0, t)|^2 \rangle = \langle |X_\varphi(\mathbf{r}, \mathbf{r}_0, t)|^2 \rangle + \langle |Y_\varphi(\mathbf{r}, \mathbf{r}_0, t)|^2 \rangle. \quad (69)$$

From there, it follows that $\varepsilon^2 = \varepsilon_{X_\varphi}^2 + \varepsilon_{Y_\varphi}^2$. One then deduces the second identity by equating $\mu = \varepsilon^2 + 2\sigma^2\alpha$ with $\mu_{X_\varphi} + \mu_{Y_\varphi} = \varepsilon_{X_\varphi}^2 + \sigma_{X_\varphi}^2\alpha + \varepsilon_{Y_\varphi}^2 + \sigma_{Y_\varphi}^2\alpha = \varepsilon^2 + (\sigma_{X_\varphi}^2 + \sigma_{Y_\varphi}^2)\alpha$. But from above, one also has that $\varepsilon_{Y_\varphi} = 0$.

V. NUMERICAL EXAMPLE

A. Materials and methods

To investigate the validity of the two conditions (36) and (37) with reasonably small values of ϵ and L_1 , we have performed simulations of the scatterers with variable levels of spatial clustering.

As in Destrempes *et al.*,⁴ we considered a resolution cell (based on an ellipsoid shape) with a semiprincipal axis in the beam direction measuring $\ell_z/2 = 0.2180$ mm and the two other semiprincipal axes measuring $\ell_x/2 = \ell_y/2 = 0.4856$ mm, thus, yielding a volume of $|V| = 0.2153$ mm³. Moreover, we adopted a center frequency $f_c = 10$ MHz and speed of sound $c_0 = 1540$ m/s, yielding a wave number of $k_c \approx 40.8$ mm⁻¹ and a wavelength of $\lambda_c = 0.1458$. The effective axial resolution was equal to $\tilde{\ell}_z/2 = 0.2310$ mm. Assuming a Gaussian-shaped PSF of the form stated in Sec. IV C and the surface of the effective resolution cell defined at -20 dB, we obtained $\sigma_x = 0.2263$, $\sigma_y = 0.2263$, and $\tilde{\sigma}_z = 0.1076$. We used these values in Eqs. (8a) and (8b), using Eq. (15). Moreover, we adopted $\alpha_n \sim \mathcal{N}(0, 1)$ in these equations. The effective resolution cell was embedded into a rectangular box R of dimension $(5 \times 0.2310) \times (5 \times 0.2310) \times (2 \times 0.2310)$ mm³.

The number N of scatterers per effective resolution cell was varied from 1 to 21 by steps of 2, whereas the packing

factor W varied from 1 to 11 by steps of 2. The expected scatterer clustering parameter, which is equal to $\alpha = N/W$, thus, varied from 1/11 to 21. For the purpose of simulating the scatterers, the circumscribing rectangular box was covered with $M_c = 15 \times 15 \times 6$ nonoverlapping small cubes, each one with side length $\delta = 0.2310/3$ mm. The desired number of scatterers was, therefore, equal to $N_p = N \times |R|/|\tilde{V}|$. Then, within each of these small cubes, the number of scatterers was sampled according to a negative binomial distribution with mean $t = N_p \times \delta^3/|R|$ and variance equal to Wt , if $W > 1$, and according to a Poisson distribution of mean t , if $W = 1$. As the sampling on each small cube was performed independently from the other cubes, within the volume encompassed by the M_c nonoverlapping cubes, one obtains a number of scatterers with a mean value equal to $M_c t$ and variance equal to $W M_c t$ (variances of independent random variables add up). Henceforth, within the rectangular box, one obtains a number of scatterers with a mean equal to N_p and variance equal to $W N_p$ as desired. The positions of the scatterers were simulated in this fashion until their number was actually equal to N_p . Furthermore, the number of uniformly distributed sample points within each spherical scatterer was sampled with a Poisson distribution of mean $M_0 = 30$, where we adopted a scatterer's radius of $2.75 \mu\text{m}$ (as for human red blood cells). For this purpose, we used the algorithm for sampling uniformly within a three-dimensional (3D) ball mentioned in Harman and Lacko.⁴⁶ The random variable U could then be calculated based on Eq. (25) using either the cosine or sine functions as in Eqs. (8a) and (8b) evaluated with Eq. (15).

The rectangular box circumscribing the effective resolution cell was partitioned into $5 \times 5 \times 2$ cubes ($M = 50$), each one with a side length equal to 0.2310. The same procedure as above was applied independently to each of these M cubes. In doing so, the number of scatterers within each of the M cubes was simulated until the total number was equal to N_p . Uniform sampling within each spherical scatterer could then be performed as above. The random variable U' was then calculated based on Eq. (26) using either the cosine or sine functions. We implemented the simulation procedure on the platform MATLAB (The MathWorks, Natick, MA, version 2018a).

For each pair of values (N, W) , $N_{\text{samp}} = 500$ samples of the variables U and U' were simulated in this fashion using either the cosine or sine functions. The Kolmogorov distance ϵ between the variables U/τ and U'/s , where we took $\tau = \sqrt{\text{Var}[U]}$ and $s = \sqrt{\sum_{m=1}^M \text{Var}[U'_m]}$ [see Eqs. (27) and (29b) in Sec. III C], was estimated with the MATLAB function “kstest2” (ignoring the output p -value). The value of L_1 was estimated from the N_{samp} samples of the variables U'_m , $m = 1, \dots, M$. The combination $\rho_0 = \epsilon + C_0 L_1$ was then viewed as an upper bound for the Kolmogorov distance between U/τ and the standard normal distribution.

We then applied the Kolmogorov-Smirnov goodness-of-fit test to assess whether the random variable U/τ is distributed according to the standard normal distribution. For

this purpose, we used a confidence level of 0.05. In the case of this hypothesis test, the p -value is equal to $\text{Prob}(\sqrt{N_{\text{samp}}}D_{N_{\text{samp}}} > \rho_0)$, where $D_{N_{\text{samp}}}$ represents the Kolmogorov-Smirnov statistic. One uses its asymptotic expression $\text{Prob}(K > \rho_0) = 1 - L(\rho_0)$ (for large values of N_{samp}), where K is the Kolmogorov distribution²⁴ with known cumulative distribution L . We implemented the calculation of the p -value as $1 - \text{Prob}(D_{N_{\text{samp}}} < \rho_0/\sqrt{N_{\text{samp}}})$ using the efficient algorithm of Marsaglia *et al.*⁴⁷ For this purpose, we used the package⁴⁸ “kolmin” of the statistical software *R* (*R* Foundation for Statistical Computing, Vienna, Austria, version 3.3.2).

B. Results

As shown in Figs. 2(a) and 2(b), conditions (36) and (37) were satisfied with the variable values of ϵ and L_1 using either Eq. (8a) or Eq. (8b), respectively. The resulting linear combination $\rho_0 = \epsilon + C_0L_1$ is also displayed in Fig. 2. The resulting p -values for the standard normal distribution hypothesis were all above 0.85 (in fact, above 0.99 for most of them). Thus, the Kolmogorov-Smirnov tests succeeded, which shows that the hypothesis $U/\tau \sim \mathcal{N}(0, 1)$ is valid under the tested conditions.

VI. DISCUSSION AND CONCLUSION

In this work, the statistical modelings of the RF signals, their Hilbert transform, and the echo envelope were presented. Notably, we have addressed the scenario of possibly spatially correlated scatterers, unlike what was previously done in the literature in the context of ultrasound signals statistical modeling. The proposed theoretical framework allowed the deduction of 1D or 2D homodyned K-distribution models for the RF signals or the echo envelope, respectively. In particular, a physical interpretation of the homodyned-K scatterer clustering parameter α could be derived in this framework, which is related to the packing factor appearing in quantitative spectral analysis.

The special case of the K-distribution was previously proposed to model the absolute value of the RF signals in Bernard *et al.*⁷ Here, we have generalized this model to take into account a possibly nonvanishing coherent component. However, notice that in the case of a phase shift of $\varphi = \pi/2$ in the emitted signal of Eq. (7), the case of a K-distribution does apply. The phase shift φ , which is a characteristic of the emitted signal and was considered in Sec. II A, is crucial in decomposing the analytic signal $\text{RF} + i\mathcal{H}(\text{RF})$ in the form $(X_\varphi + iY_\varphi)e^{i\varphi}$ as in Eq. (7), where X_φ is distributed according to a 1D homodyned K-distribution, whereas Y_φ is distributed according to a 1D K-distribution.

In Eq. (17) of Chen *et al.*,¹⁶ in the case of several independent scatterers, it is shown that parameter α is expected to be the same for both of the RF signals and their echo envelope, which is consistent with the proposed theoretical framework, under which the three distributions in Eqs. (45), (47), and (67) share the same parameter α .

In the presence of specular reflection, due to the presence of scatterers larger than the wavelength, Secs. 8.3 and 8.4 in Morse and Ingard³⁵ suggest that the demodulated analytic complex signal will be of the form $\epsilon_{sp}e^{-i\tilde{k}cz}$, which implies that a constant $\langle \epsilon_{sp} \rangle$ has to be added to the coherent component of the 2D homodyned K-distribution. Furthermore, in the case where the phase shift φ is equal to zero, one may assume that the Hilbert transform of the RF signals is distributed according to a K-distribution even in the presence of specular reflection but otherwise not.

Notice that the in-phase/quadratic (IQ) signal is obtained by performing demodulation around the center frequency f_c rather than the nominal center frequency \tilde{f}_c , the latter resulting from the usual downshifting due to the ultrasound attenuation caused by the intervening tissues. However, this choice does not affect the echo envelope because the latter is the modulus of the (modulated or not) analytic complex signal. Nonetheless, we chose demodulation around the nominal center frequency for the purpose of expressing the analytic signal in a form that is amenable to the proposed statistical modeling. Indeed, after demodulation around the center frequency and

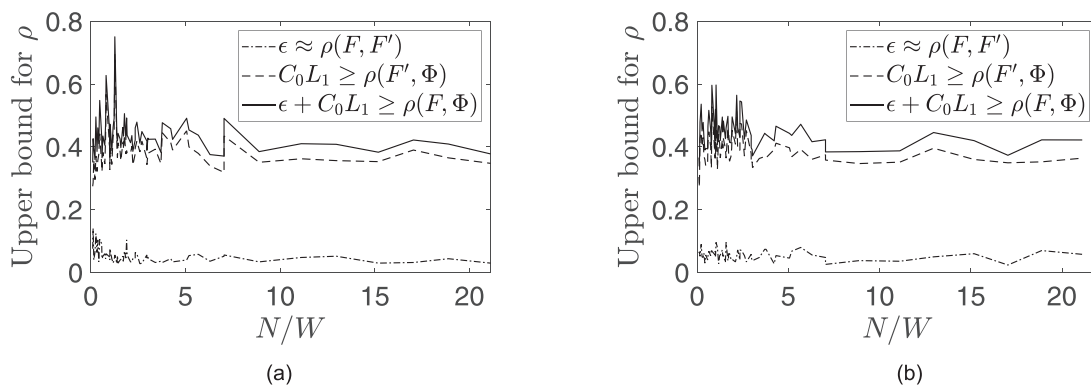


FIG. 2. (a) The goodness-of-fit results on simulations of $N_{\text{samp}} = 500$ samples of the variables U and U' using Eqs. (8a) and (15) with $M = 50$. ϵ is the estimate for the Kolmogorov distance $\rho(F, F')$ between U/τ and U'/s as computed with the empirical distance between $U/\sqrt{\text{Var}[U]}$ and $U'/\sqrt{\text{Var}[U']}$; C_0L_1 denotes the upper bound for the Kolmogorov distance $\rho(F', \Phi)$ between U'/s and $\mathcal{N}(0, 1)$, as computed with the left-hand side of the condition Eq. (37); the combination $\rho_0 = \epsilon + C_0L_1$ is then an upper bound for $\rho(F, \Phi)$. (b) The results are shown similarly when using Eqs. (8b) and (15).

compensation of the phase shift in the transmitted voltage, one obtains the two components in Eqs. (8a) and (8b), and the second component is distributed according to a 1D K-distribution.

Note that different values of W are achievable for a given number density of randomly (but possibly non-uniformly) positioned scatterers because the spatial correlation between the scatterers' positions may occur in a stochastic point process at various degrees. It follows that the tissue characterization may be reached through estimates of W or α as these two stochastic parameters yield a signature of the tissues scatterers' spatial organization. It is noteworthy that both parameters reveal information on the scatterers' organization at a scale (possibly much) smaller than the wavelength.

We have not pursued the case of periodically spaced scatterers in this work, but nevertheless the notion of the packing factor was considered as a means of quantifying the scatterers' spatial organization. Future works could also include this feature, although it does not seem to be as crucial as other aspects in view of the clinical applications.

In our previous work,⁶ we had tested the conjectured interpretation $\alpha = m|V|/W$ on simulated ultrasound images. In the current study, we have refined this interpretation by considering a product of two factors 0.7609 and $\tilde{\ell}_z/\ell_z$ [cf. Eq. (57)], where $\tilde{\ell}_z/\ell_z > 1$, thus, allowing for an adjustment depending on the data. Whereas the second factor is imposed by the condition of uncorrelated real and imaginary parts of the analytic signal, the first factor follows from the consideration of Chen *et al.*,¹⁶ albeit this work was developed under the hypothesis of independent scatterers. In a future study, we intend to validate our choice of this constant in the context of clustered scatterers based on simulated ultrasound images.

In future works, it would be interesting to study the effect of post-processed filtering on the remaining parameters of the homodyned K-distribution, which, in principle, could allow the picking up of information on the backscatter coefficient at different frequencies and characteristic changes in the spectral slope depending on the scatterers' properties, number density, and spatial organization.

The approach based on sample backscattering points, which is presented in Sec. III A is akin to the sampling methods²⁵ for solving inverse scattering problems, notably the linear sampling method of Colton and Kirsch⁴⁹ and the factorization method of Kirsch.⁵⁰ It would be exciting to investigate the approach presented in this study in the field of electromagnetic scattering or any other scattering phenomena such as those mentioned in the Introduction.

ACKNOWLEDGMENTS

This work was supported by the Natural Sciences and Engineering Research Council of Canada (Grant No. 503381-16). We thank an anonymous reviewer for pointing out the relation of this work with the scattering inverse problems and suggesting a few references.

¹R. D. Lord, "The use of the Hankel transform in statistics. I," *Biometrika* **41**, 44–55 (1954).
²E. Jakeman, "On the statistics of K-distributed noise," *J. Phys. A* **13**, 31–48 (1980).
³E. Jakeman and R. J. A. Tough, "Generalized k distribution: A statistical model for weak scattering," *J. Opt. Soc. Am. A* **4**, 1764–1772 (1987).
⁴F. Destrempes, J. Porée, and G. Cloutier, "Estimation method of the homodyned K-distribution based on the mean intensity and two log-moments," *SIAM J. Imaging Sci.* **6**, 1499–1530 (2013).
⁵V. Dutt and J. F. Greenleaf, "Ultrasound echo envelope analysis using a homodyned K distribution signal model," *Ultrason. Imaging* **16**, 265–287 (1994).
⁶F. Destrempes and G. Cloutier, "Interpretation based on stochastic geometry of homodyned-K distribution scatterer clustering parameter for quantitative ultrasound imaging," in *2020 IEEE International Ultrasonics Symposium (IUS)* (September 8–11, 2020), pp. 1–4.
⁷O. Bernard, J. D'hooge, and D. Friboulet, "Statistics of the radio-frequency signal based on K distribution with applications to echocardiography," *IEEE Trans. Ultrason. Ferroelectr. Freq. Control.* **53**, 1689–1694 (2006).
⁸F. Destrempes, E. Franceschini, F. T. H. Yu, and G. Cloutier, "Unifying concepts of statistical and spectral quantitative ultrasound techniques," *IEEE Trans. Med. Imaging* **35**, 488–500 (2016).
⁹F. Destrempes and G. Cloutier, "A critical review and uniformized representation of statistical distributions modeling the ultrasound echo envelope," *Ultrasound Med. Biol.* **36**, 1037–1051 (2010).
¹⁰M. L. Oelze and J. Mamou, "Review of quantitative ultrasound: Envelope statistics and backscatter coefficient imaging and contributions to diagnostic ultrasound," *IEEE Trans. Ultrason. Ferroelectr. Freq. Control.* **63**, 336–351 (2016).
¹¹M. Gesnik, M. Bhatt, M.-H. Roy-Cardinal, F. Destrempes, L. Allard, B. N. Nguyen, T. Alquier, J.-F. Giroux, A. Tang, and G. Cloutier, "In vivo ultrafast quantitative ultrasound and shear wave elastography imaging on farm-raised duck livers during force feeding," *Ultrasound Med. Biol.* **46**, 1715–1726 (2020).
¹²V. Twersky, "Low-frequency scattering by correlated distributions of randomly oriented particles," *J. Acoust. Soc. Am.* **81**, 1609–1618 (1987).
¹³H. S. Green, *The Molecular Theory of Fluids* (Dover, New York, 1969), Chap. III, pp. 62–64.
¹⁴R. K. Saha, E. Franceschini, and G. Cloutier, "Assessment of accuracy of the structure-factor-size-estimator method in determining red blood cell aggregate size from ultrasound spectral backscatter coefficient," *J. Acoust. Soc. Am.* **129**, 2269–2277 (2011).
¹⁵P. M. Shankar, "A model for ultrasonic scattering from tissues based on the K-distribution," *Phys. Med. Biol.* **40**, 1633–1649 (1995).
¹⁶J. F. Chen, J. A. Zagzebski, and E. L. Madsen, "Non-Gaussian versus non-Rayleigh statistical properties of ultrasound echo signals," *IEEE Trans. Ultrason. Ferroelectr. Freq. Control.* **41**, 435–440 (1994).
¹⁷D. Savéry and G. Cloutier, "A point process approach to assess the frequency dependence of ultrasound backscattering by aggregating red blood cells," *J. Acoust. Soc. Am.* **110**, 3252–3262 (2001).
¹⁸F. T. H. Yu and G. Cloutier, "Experimental ultrasound characterization of red blood cell aggregation using the structure factor size estimator," *J. Acoust. Soc. Am.* **122**, 645–656 (2007).
¹⁹E. Franceschini, F. T. H. Yu, F. Destrempes, and G. Cloutier, "Ultrasound characterization of red blood cell aggregation with intervening attenuating tissue-mimicking phantoms," *J. Acoust. Soc. Am.* **127**, 1104–1115 (2010).
²⁰F. Destrempes and G. Cloutier, "Review of envelope statistics models for quantitative ultrasound imaging and tissue characterization," in *Quantitative Ultrasound in Soft Tissues*, edited by J. Mamou and M. L. Oelze (Springer, New York, 2013), Chap. 10, pp. 219–274.
²¹X. Chen, D. Phillips, K. Q. Schwarz, J. G. Mottley, and K. J. Parker, "The measurement of backscatter coefficient from a broadband pulse-echo system: A new formulation," *IEEE Trans. Ultrason. Ferroelectr. Freq. Control.* **44**, 515–525 (1997).
²²P. Billingsley, *Probability and Measure*, 3rd ed. (Wiley, New York, 1995), Chap. 5, pp. 359–367.
²³I. Shevtsova, "On the absolute constants in Nagaev-Bikelis-type inequalities," in *Inequalities and Extremal Problems in Probability and Statistics*, edited by I. Pinelis (Academic, Cambridge, MA, 2017), Chap. 3, pp. 47–102.

- ²⁴A. Kolmogorov, “Sulla determinazione empirica di una legge di distribuzione” (“On the empirical determination of a distribution law”), *G. Inst. Ital. Attuari.* **4**, 83–91 (1933).
- ²⁵D. Colton and R. Kress, “Looking back on inverse scattering theory,” *SIAM Rev.* **60**, 779–807 (2018).
- ²⁶F. Hagemann, T. Arens, T. Becke, and F. Hettlich, “Solving inverse electromagnetic scattering problems via domain derivatives,” *Inverse Probl.* **35**, 084005 (2019).
- ²⁷X. Cao, H. Diao, H. Liu, and J. Zou, “On novel geometric structures of Laplacian eigenfunctions in \mathbb{R}^3 and applications to inverse problems,” *SIAM J. Math. Anal.* **53**, 1263–1294 (2021).
- ²⁸H. Diao, H. Liu, L. Zhang, and J. Zou, “Unique continuation from a generalized impedance edge-corner for Maxwell’s system and applications to inverse problems,” *Inverse Probl.* **37**, 035004 (2021).
- ²⁹H. Diao, X. Cao, and H. Liu, “On the geometric structures of transmission eigenfunctions with a conductive boundary condition and applications,” *Commun. Partial Differ. Equations* **46**, 630–679 (2021).
- ³⁰F. Qu, B. Zhang, and H. Zhang, “A novel integral equation for scattering by locally rough surfaces and application to the inverse problem: The Neumann case,” *SIAM J. Sci. Comput.* **41**, A3673–A3702 (2019).
- ³¹M. V. Klibanov, D. L. Nguyen, and L. H. Nguyen, “A coefficient inverse problem with a single measurement of phaseless scattering data,” *SIAM J. Appl. Math.* **79**, 1–27 (2019).
- ³²X. Ji and X. Liu, “Inverse elastic scattering problems with phaseless far field data,” *Inverse Probl.* **35**, 114004 (2019).
- ³³V. A. Khoa, G. W. Bidney, M. V. Klibanov, L. H. Nguyen, L. H. Nguyen, A. J. Sullivan, and V. N. Astratov, “Convexification and experimental data for a 3D inverse scattering problem with the moving point source,” *Inverse Probl.* **36**, 085007 (2020).
- ³⁴X. Chen, Z. Wei, M. Li, and P. Rocca, “A review of deep learning approaches for inverse scattering problems (invited review),” *Prog. Electromagn. Res.* **167**, 67–81 (2020).
- ³⁵P. M. Morse and K. U. Ingard, *Theoretical Acoustics* (Princeton University Press, Princeton, NJ, 1968), Chap. 8, pp. 411, 441–442, and 449.
- ³⁶D. Colton and P. Monk, “The inverse scattering problem for acoustic waves in an inhomogeneous medium,” *Quart. J. Mech. Appl. Math.* **41**, 97–125 (1988).
- ³⁷A. D. Pierce, *Acoustics: An Introduction to Its Physical Principles and Applications*, 3rd ed. (Springer Nature Switzerland AG, Cham, Switzerland, 2019), Chap. 1, pp. 20–21, and Chap. 9, pp. 494–495.
- ³⁸M. F. Insana, R. F. Wagner, D. G. Brown, and T. J. Hall, “Describing small-scale structure in random media using pulse-echo ultrasound,” *J. Acoust. Soc. Am.* **87**, 179–192 (1990).
- ³⁹J. Ng, R. Prager, N. Kingsbury, G. Treece, and A. Gee, “Modeling ultrasound imaging as a linear, shift-variant system,” *IEEE Trans. Ultrason. Ferroelectr. Freq. Control.* **53**, 549–563 (2006).
- ⁴⁰S. D. Pye, S. R. Wild, and W. N. McDicken, “Adaptive time gain compensation for ultrasonic imaging,” *Ultrasound Med. Biol.* **18**, 205–212 (1992).
- ⁴¹T. A. Bigelow and Y. Labyed, “Attenuation compensation and estimation,” in *Quantitative Ultrasound in Soft Tissues*, edited by J. Mamou and M. L. Oelze (Springer, New York, 2013), Chap. 4, pp. 71–93.
- ⁴²R. de Monchy, F. Destrepes, R. Saha, G. Cloutier, and E. Franceschini, “Coherent and incoherent ultrasound backscatter from cell aggregates,” *J. Acoust. Soc. Am.* **140**, 2173–2184 (2016).
- ⁴³S. A. Frank and E. Smith, “A simple derivation and classification of common probability distributions based on information symmetry and measurement scale,” *J. Evol. Biol.* **24**, 469–484 (2011).
- ⁴⁴J. A. Rice, *Mathematical Statistics and Data Analysis*, 3rd ed. (Duxbury, Belmont, CA, 2006), Chap. 2, pp. 40–41, and Chap. 8, pp. 302–305.
- ⁴⁵M. Greenwood and G. U. Yule, “An inquiry into the nature of frequency distributions representative of multiple happenings with particular reference of multiple attacks of disease or of repeated accidents,” *J. R. Stat. Soc.* **83**, 255–279 (1920).
- ⁴⁶R. Harman and V. Lacko, “On decompositional algorithms for uniform sampling from n -spheres and n -balls,” *J. Multivar. Anal.* **101**, 2297–2304 (2010); see p. 2298 (lines 3–7).
- ⁴⁷G. Marsaglia, W. W. Tsang, and J. Wang, “Evaluating Kolmogorov’s distribution,” *J. Stat. Softw.* **8**, 1–4 (2003).
- ⁴⁸L. Carvalho, “An improved evaluation of Kolmogorov’s distribution,” *J. Stat. Softw., Code Snippets* **65**, 1–8 (2015).
- ⁴⁹D. Colton and A. Kirsch, “A simple method for solving inverse scattering problems in the resonance region,” *Inverse Probl.* **12**, 383–393 (1996).
- ⁵⁰A. Kirsch, “Factorization of the far field operator for the inhomogeneous medium case and an application to inverse scattering theory,” *Inverse Probl.* **15**, 413–429 (1999).